**Author(s):** Fachada, Vasco; Rahkila, Paavo; Fachada, Nuno; Turpeinen, Tuomas; Kujala, Urho M.; Kainulainen, Heikki

**Title:** Enlarged PLIN5-uncoated lipid droplets in inner regions of skeletal muscle type II fibers associate with type 2 diabetes

**Year:** 2022

**Version:** Published version

Acta Histochemica 124 (2022) 151869

Contents lists available at ScienceDirect

Acta Histochemica

journal homepage: www.elsevier.com/locate/acthis

# Enlarged PLIN5-uncoated lipid droplets in inner regions of skeletal muscle type II fibers associate with type 2 diabetes

Vasco Fachada [a,*], Paavo Rahkila [a], Nuno Fachada [b], Tuomas Turpeinen [c], Urho M. Kujala [a], Heikki Kainulainen [a]

[a] Faculty of Sport and Health Sciences, NeuroMuscular Research Center, University of Jyvaskyla, Rautpohjankatu 8, Jyvaskyla 40014, Finland
[b] Lusofona University, COPELABS, Lisboa 1749-024, Portugal
[c] Department of Physics, University of Jyvaskyla, Jyvaskyla 40014, Finland

ARTICLE INFO

*Keywords:*
Lipid droplets
PLIN5
Type II diabetes
Skeletal muscle
Insulin resistance
Fiber type

ABSTRACT

Skeletal muscle physiology remains of paramount importance in understanding insulin resistance. Due to its high lipid turnover rates, regulation of intramyocellular lipid droplets (LDs) is a key factor. Perilipin 5 (PLIN5) is one of the most critical agents in such regulation, being often referred as a protector against lipotoxicity and consequent skeletal muscle insulin resistance. We examined area fraction, size, subcellular localization and PLIN5 association of LDs in two fiber types of type 2 diabetic (T2D), obese (OB) and healthy (HC) individuals by means of fluorescence microscopy and image analysis. We found that T2D type II fibers have a significant sub-population of large and internalized LDs, uncoated by PLIN5. Based on this novel result, additional hypotheses for the pathophysiology of skeletal muscle insulin resistance are formulated, together with future research directions.

## 1. Introduction

Skeletal muscle is a specialized tissue with particular importance in mammalian physiology, from energy turnover to a wide range of signaling pathways and consequent metabolic and health implications, such as insulin resistance (Coen et al., 2009; Goodpaster and Wolf, 2004; LeLay and Dugail, 2009; Machann et al., 2004). In the past two decades, the understanding of such roles has been strengthened by the uprising study of lipid droplets (LDs) as a key role player in cell signaling, including its relationship to insulin resistance. Initially it was thought this relationship was linear, where increased intramyocellular lipid content (IMCL) translated directly into elevated insulin resistance. Later, however, the so called *atlhete's paradox* demonstrated that extremely insulin sensitive individuals, such as endurance athletes, had even higher IMCL than type 2 diabetic patients (Goodpaster et al., 2001; Van Loon et al., 2004; van Loon and Goodpaster, 2006; Moro et al., 2008). Such data shifted research from quantitative towards more qualitative facets of IMCL regulation, namely lipotoxicity, i.e., the hypothesis that byproducts from inefficient IMCL lipolysis could trigger insulin resistance signaling (Russell, 2004).

One of the hot topics became the Perilipin (PLIN) family, a group of proteins directly involved in LDs turnover by often coating these organelles and regulating the access of enzymes and related co-activators (Bickel et al., 2009; MacPherson and Peters, 2015; Minnaard et al., 2009). One of the PLIN members, PLIN5, is known to express significantly in highly oxidative tissues, as skeletal muscle (Wolins et al., 2006). Given PLIN5's significant participation in IMCL physiology, it has become one of the central agents in the study of skeletal muscle insulin resistance, namely by its function in protecting against lipotoxicity (Mason and Watt, 2015; Gemmink et al., 2016). Moreover, together with fiber typing, subcellular localization of IMCL has also been studied in relation to insulin resistance and muscle oxidative capacity (Nielsen et al., 2010; Shaw et al., 2008, 2009, 2020; Koh et al., 2018).

Nevertheless, we believe that LDs sub-populations have yet to be fully identified, namely concerning the relationship between their size, subcellular localization and PLIN5 association. We hence hypothesized that the relationship between intramyocellular LDs and PLIN5 in different fiber types would reveal hidden profile differences between

*Abbreviations:* LDs, lipid droplets; all-LDs, all lipid droplets; col-LDs, colocalized lipid droplets; unc-LDs, uncoated lipid droplets; HC, healthy controls; OB, obese; T2D, type II diabetic; IMCL, intramyocellular lipids; PLIN5, perilipin 5.

* Corresponding author.
*E-mail address:* vasco.fachada@jyu.fi (V. Fachada).

https://doi.org/10.1016/j.acthis.2022.151869
Received 19 October 2021; Received in revised form 3 February 2022; Accepted 12 February 2022
Available online 24 February 2022

healthy and insulin resistant individuals. Thus, we analyzed microscope images of human skeletal muscle of type 2 diabetic (T2D), obese (OB) and healthy control (HC) human subjects. We explored two different fiber types for area fraction, size and subcellular localization of LDs, PLIN5 and their colocalization. Subtle key differences in skeletal muscle lipid profile were found between the studied groups and novel observations were made concerning IMCL and its relationship with PLIN5 in different fiber types.

## 2. Methods

### 2.1. Subjects

Twenty-five physically inactive male individuals were divided into three groups according to their health status and weight. Seven healthy, non-diabetic subjects (BMI $\leq$ 30 kg.m$^{-2}$ or body fat percentage 10–20%) were included in the HC. The obese group consisted of 8 non-diabetic obese subjects (BMI $>$ 30 kg.m$^{-2}$). The type II diabetic group consisted of 10 subjects clinically diagnosed with type 2 diabetes (Table 1). Most individuals in T2D were medicated against insulin resistance and/or high blood pressure. Written informed consent and health questionnaires were obtained from all volunteers before starting any measurements. The study plan was approved by the ethical committee of the University of Jyväskylä.

Blood samples were collected from the brachial artery after overnight fasting. All blood variables were measured in plasma by standard enzymatic methods using Roche Diagnostic's reagents with an automated analyzer (Roche Modular P800, Roche Diagnostics GmbH, Germany).

Maximal oxygen consumption ($VO_2$ max) was measured in a graded bicycle test. Respiratory gases were measured by open-circuit spirometry (Oxycon Pro Jæger, Germany). The test was carried until subjects wanted to stop, or when heart rate, blood pressure or oxygen consumption started decreasing. The maximal oxygen consumption was considered as the highest 30 s average of oxygen consumption in relative value (mL.min$^{-1}$.kg$^{-1}$).

Prior to collecting the muscle biopsy, subjects refrained from physical exercise for 48 h. Before taking the biopsy the skin area was shaved and cooled with ice for ten minutes before local the anesthetic was injected (Lidocain 20 mg.mL$^{-1}$ c. adrenalin). The biopsy was performed with a Bergström needle from the vastus lateralis muscle approximately 15 cm above the patella tendon and 2 cm away from the fascia. The samples were covered with Tissue-Tek and frozen immediately in isopentane cooled with liquid nitrogen, then finally stored at − 80°C until further analyses.

### 2.2. Histology and imaging

Five micrometer cross sections were cut in a cryostat at − 25°C (Leica CM 3000, Germany). Sections were collected in 13 mm round coverslips and immediately fixed in 4% paraformaldehyde for 15 min at room temperature (RT).

**Table 1**
Group characteristics. Mean ± SEM. ** $P < 0.01$ using a Kruskal-Wallis H test. Pairwise post hoc significance ($P < 0.05$) is denoted with letters *a* to *c*, from highest to lowest value.

| | Controls (HC) | Diabetic (T2D) | Obese (OB) |
|---|---|---|---|
| n | 7 | 10 | 8 |
| Age (years) | 56.4 ± 2.8 | 52.7 ± 2.2 | 51.9 ± 3.2 |
| Body weight (kg)** | 78.4 ± 2.4$^{c}$ | 112.0 ± 7.1$^{a}$ | 99.6 ± 5.4$^{b}$ |
| BMI (kg.m$^{-2}$)** | 25.8 ± 0.4$^{b}$ | 34.0 ± 1.6$^{a}$ | 32.3 ± 1.0$^{a}$ |
| Fat percentage (%)** | 19.9 ± 1.1$^{b}$ | 29.2 ± 1.4$^{a}$ | 30.7 ± 1.8$^{a}$ |
| Tryglycerides (mmol.L$^{-1}$)** | 1.4 ± 0.2$^{b}$ | 2.8 ± 0.7$^{a}$ | 1.8 ± 0.4$^{b}$ |
| Blood glucose (mmol.L$^{-1}$)** | 5.1 ± 0.2$^{b}$ | 8.0 ± 1.3$^{a}$ | 5.1 ± 0.6$^{b}$ |
| $VO_2$ max (mL.min$^{-1}$.kg$^{-1}$)** | 30.7 ± 1.5$^{b}$ | 23.0 ± 1.8$^{a}$ | 28.6 ± 2.1$^{b}$ |

After washing for 3×5 minutes with phosphate buffer saline (PBS), the sections were blocked with 3% bovine serum albumin (BSA) for 30 min and then washed briefly with PBS. Primary antibodies were diluted in 1% BSA and incubated for 1 h in at RT, using GP31 (Progen, Germany) against PLIN5 diluted 1–200 and M4276 (Sigma, USA) against fast myosin heavy chain diluted 1–50.

Next, the samples were washed for 3×15 min with PBS, before incubating with the secondary antibodies in 1% BSA for 1 h in dark RT, using anti guinea pig IgG AlexaFluor 594 (JacksonImmunoResearch, USA) diluted 1–50 together with anti mouse IgG AlexaFluor AMCA (JacksonImmunoResearch, USA) diluted 1–50. A 3×10 min PBS washing followed. Up to this point, all steps were performed with 0.05% saponin. Lipid droplets were then stained with LipidTOX™ Green (FITS, Molecular Probes), using a 1–100 dilution in PBS for 30 min in dark RT. Excess dye was removed with 2×10 seconds brief PBS wash right before mounting.

Slides were mounted using Mowiol with 2.5% DABCO (Sigma-Aldrich) and left to dry for at least 1 h in the dark at 4°C.

Raw data collection was achieved with a BX50 BXFLA (Olympus, Japan), coupled to ColorViewIII camera (Soft Imaging Systems), through a 40x/0.75NA objective. Fluorophores were excited with a mercury lamp, through U-MWU, U-MWB and MWG excitation cubes. Controlled with the software AnalySIS 5.0 (Soft Imaging Systems), fluorescent signal was gray-scale recorded for each channel. Fig. 1a-c represents raw data prior to any image processing.

### 2.3. Image processing and variable assessment

Fluorescent 0.5 $\mu$m microspheres (TetraSpeck, Molecular Probes) were used for particle size calibration and exclusion of diffracted signal as illustrated in Fig. 1D-I. Prior to analyses, all images were denoised and deconvoluted in *ImageJ* (Schneider et al., 2012) using a theoretical point spread function separately for each channel.

From each cross section, all intact and artifact-free skeletal muscle fibers were selected, and then carefully segmented (HC = 88 ± 20; T2D = 32 ± 7 and OB = 41 ± 9. Mean ± SE). Cells were classified into either type I or type II fibers, according to the detected and thresholded signal of fast myosin per cell area (cutoff value = 500). For each cell, every binarized particle (Fig. 1F) was measured in *ImageJ*. Size and subcellular localization of each of these particles was assessed in different fiber types. These variables were measured from the total number of detected LDs (all-LDs), PLIN5, the LDs associating with PLIN5 (col-LDs), and for the LDs uncoated with PLIN5 (unc-LDs). The association between PLIN5 and LDs was determined by colocalization (Costes et al., 2004) and performed as previously (Nissinen et al., 2021).

### 2.4. Data analysis

Unless stated otherwise, significance between the three groups (marked with *) and fiber types (marked with #) was assessed with two-way analysis of variance (ANOVA2). For post hoc analysis to compare fiber type differences between each group or any variable between two given groups, Mann-Whitney U test was performed. Normality was assessed with Shapiro-Wilk test and histogram inspection. Boxes in the boxplot figures depict interquartile ranges and medians, while whisquers represent the 95% confidence interval. Correlation analyses were carried with Spearman's $\rho$. Statistical significance levels were set at $P < 0.05$ and $P < 0.01$. Data crunching, statistics and visualization were performed in *Python*, with the packages *NumPy* (Harris et al., 2020), *pandas* (Anon, 2020), *SciPy* (Virtanen et al., 2020), *statsmodels* (Seabold and Perktold, 2010), *seaborn* (Waskom, 2020) and *matplotlib* (Hunter, 2007), respectively. All *ImageJ* and *Python* routines can be found at https://github.com/seiryoku-zenyo/Diabetic-study.

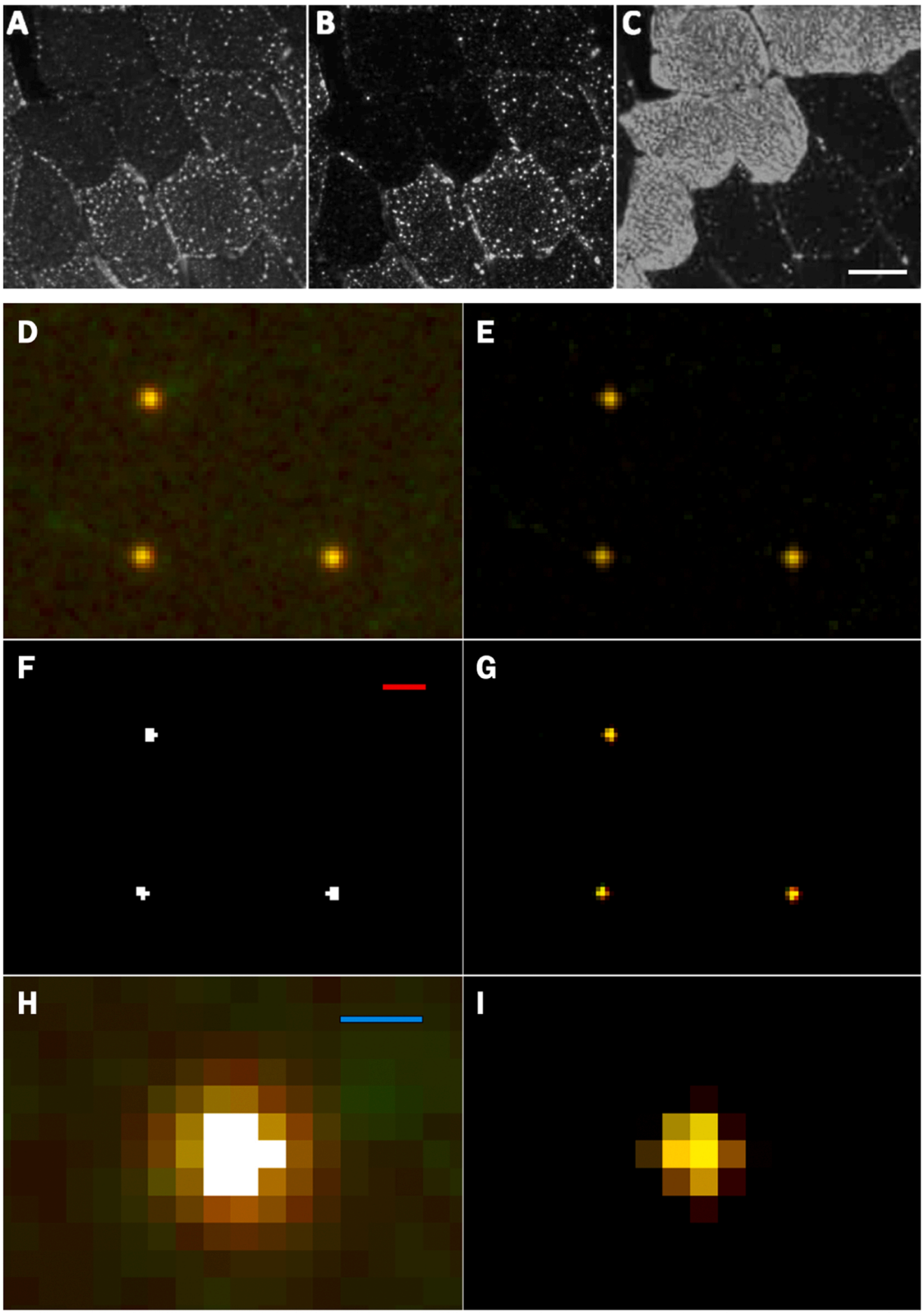


**Fig. 1.** Microscope data calibration. A): LipidTOX. B): PLIN5. C): Fast myosin. D): Raw imaged 0.5 $\mu$m microspheres. E): Denoising of D. F): Binarization ("Otsu" threshold) of G. G) Deconvolution (Richardson-Lucy) of E. H): Cropping of upper left microsphere, binarized data (F) overlayed on raw data (D). I): Cropping of deconvoluted upper left microsphere (G). White bar in C = 40 $\mu$m, red bar in F = 2 $\mu$m, blue bar in H = 0.5 $\mu$m.

## 3. Results

### 3.1. Area fraction

Despite the visible tendency of increased IMCL in T2D and OB, no significant differences between groups were detected in all-LDs fraction. Nonetheless, amongst groups and as expected, type I fibers showed significantly higher all-LDs fraction when compared to type II fibers ($P = 0.05$). Such fiber type differences were mainly driven by differences within the HC and T2D groups ($P = 0.02$ and $P = 0.032$, respectively), as seen in Fig. 2a.

Interestingly, however, concerning unc-LDs area fraction, HC retained fiber type differences ($P = 0.048$), while T2D lost these differences ($P = 0.24$). Consequently, type II fibers of T2D showed significantly higher unc-LD area fraction than the same fiber type in HC ($P = 0.044$) as seen in Fig. 2c.

More clearly than in all-LDs, we found significant differences in PLIN5 area fraction between fiber types amongst groups ($P = 1.01e^{-9}$) and within every group ($P = 0.001$ for HC, $P = 1e^{-4}$ for T2D and $P = 0.041$ for OB), as seen in Fig. 2d. The increased PLIN5 area fraction in type I fibers was especially evident in T2D, where post hoc revealed significantly higher values versus the same fiber type in HC ($P = 0.029$). It is interesting to note that the same increased PLIN5 area fraction in Type I fibers of T2D versus HC, was not observed between type II fibers of both groups ($P = 0.20$).

In addition to higher PLIN5 area fraction in type I fibers, T2D also showed significantly higher fraction of col-LDs than HC in both fiber types ($P = 0.014$ for type I fibers and $P = 0.036$ for type II fibers) as seen in Fig. 2b.

### 3.2. LD diameter

In terms of LD size, we found significant differences in the diameter of all-LDs between groups ($P = 0.008$), especially in type II fibers ($P = 0.021$). As summarized by Fig. 3a, these differences were mainly driven by larger all-LDs in T2D versus HC ($P = 0.029$ for type I fibers and $P = 0.001$ for type II fibers).

Although ANOVA2 showed no fiber type differences amongst all groups, we did find that T2D alone had significantly larger all-LDs in type II fibers in comparison to type I fibers ($P = 0.027$). Interestingly, these differences in LD size seem to originate from unc-LDs ($P = 0.027$) and not from col-LDs, where differences between fiber types disappear ($P = 0.76$), as presented in Fig. 3b-c.

As expected, col-LDs were significantly larger than unc-LDs in both fiber types of all groups ($P < 0.01$).

### 3.3. Subcellular localization

The HC group showed a tendency for all-LDs being closer to the sarcolemma as seen in Fig. 4a, albeit no differences with ANOVA2 between groups ($P = 0.12$) or fiber types ($P = 0.3$). Unlike the other groups however, HC showed closer all-LDs to sarcolemma in type II fibers when compared to type I ($P = 0.027$). Interestingly, HC type II fibers revealed significantly closer all-LDs to the sarcolemma versus the same fiber type in T2D ($P = 0.018$). Again, the internalized nature of all-LDs seem to originate from unc-LDs (Fig. 4c).

It is worth noting that ANOVA2 did show PLIN5 to be significantly closer to the sarcolemma in type II fibers ($P = 0.032$), albeit not detecting significant differences between groups ($P = 0.07$), as highlighted in Fig. 4d.

### 3.4. Diameter versus localization

Given the increased fraction and size of unc-LDs, together with its deeper subcellular localization in type II fibers of T2D, we decided to further investigate such relationship.

By plotting a bivariate kernel density estimation between the diameter and subcellular location of LDs, we observed that T2D has a substantial sub-population of enlarged unc-LDs in inner regions of type II fibers only (Fig. 5b).

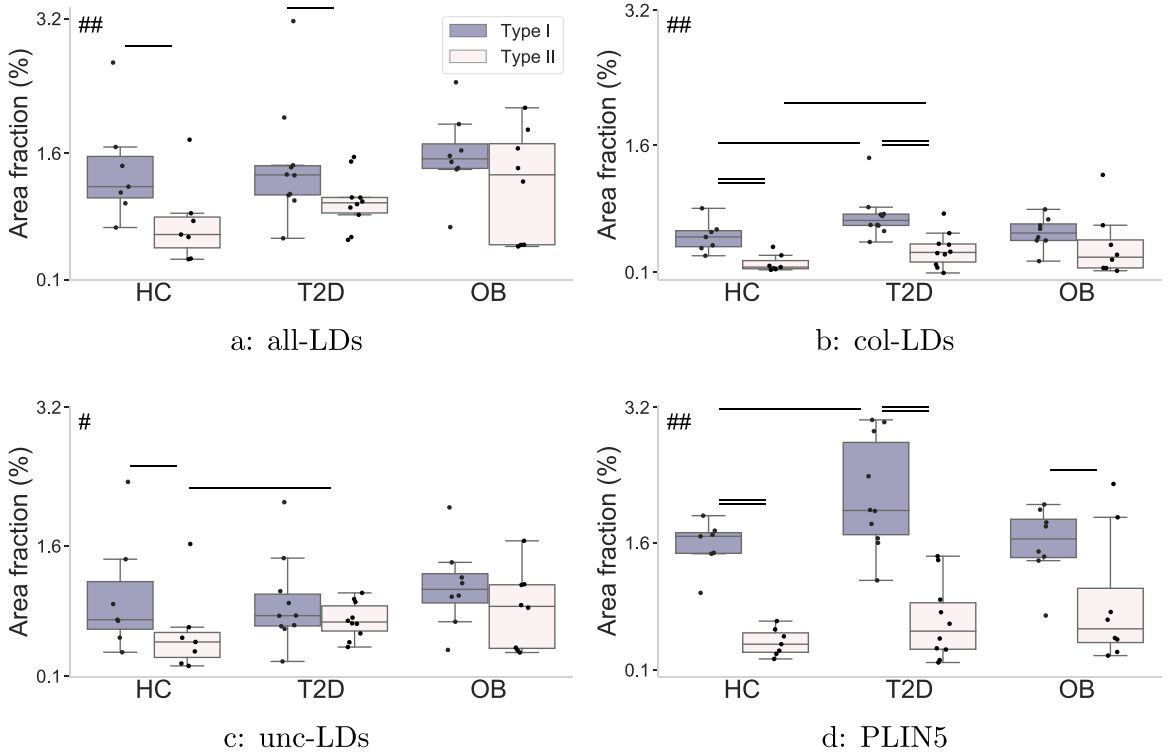


**Fig. 2.** Area fraction for a) all-LDs; b) col-LDs; c) unc-LDs and d) PLIN5. Fiber type differences by ANOVA2 denoted with #($P < 0.05$) and ##($P < 0.01$). Post hoc statistical significance is denoted with horizontal bars ($P < 0.05$) or double horizontal bars ($P < 0.01$).

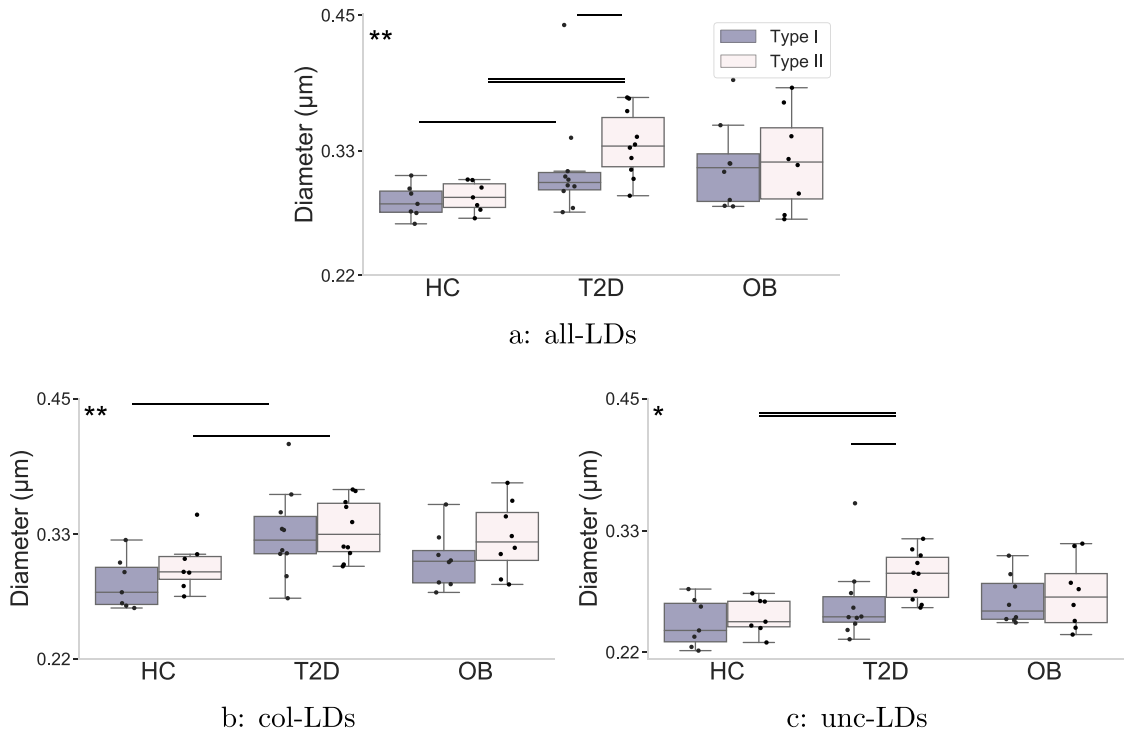


**Fig. 3.** Size of a) all-LDs; b) col-LDs and c) unc-LDs. Group differences by ANOVA2 denoted with * ($P < 0.05$) and **($P < 0.01$). Post hoc statistical significance is denoted with horizontal bars ($P < 0.05$) or double horizontal bars ($P < 0.01$).

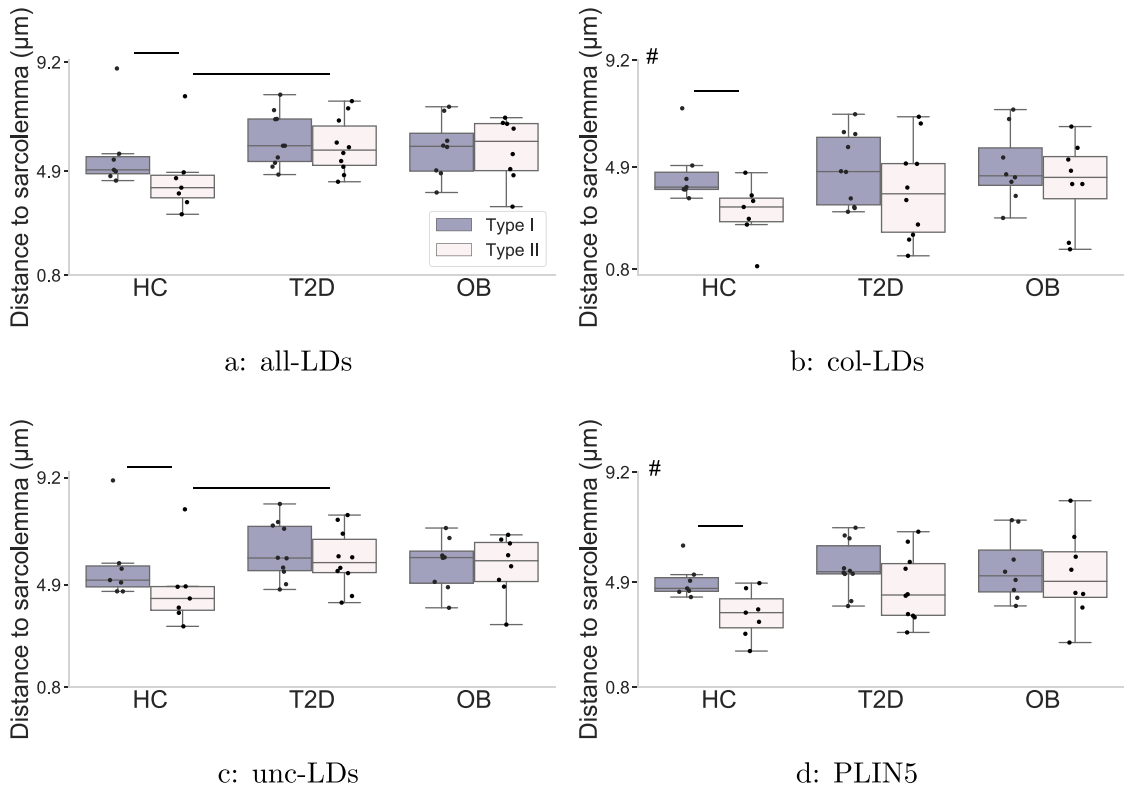


**Fig. 4.** Distance to sarcolemma of a) all-LDs; b) col-LDs; c) unc-LDs and d) PLIN5. Fiber type differences by ANOVA2 denoted with #($P < 0.05$). Post hoc statistical significance is denoted with horizontal bars ($P < 0.05$).

In all groups and fiber types, the largest LDs could be found associating with PLIN5 and close to the sarcolemma. This was more evident in type II fibers, where we found a relatively low density (light tones) of col-LDs in inner regions of the cells (Fig. 5a).

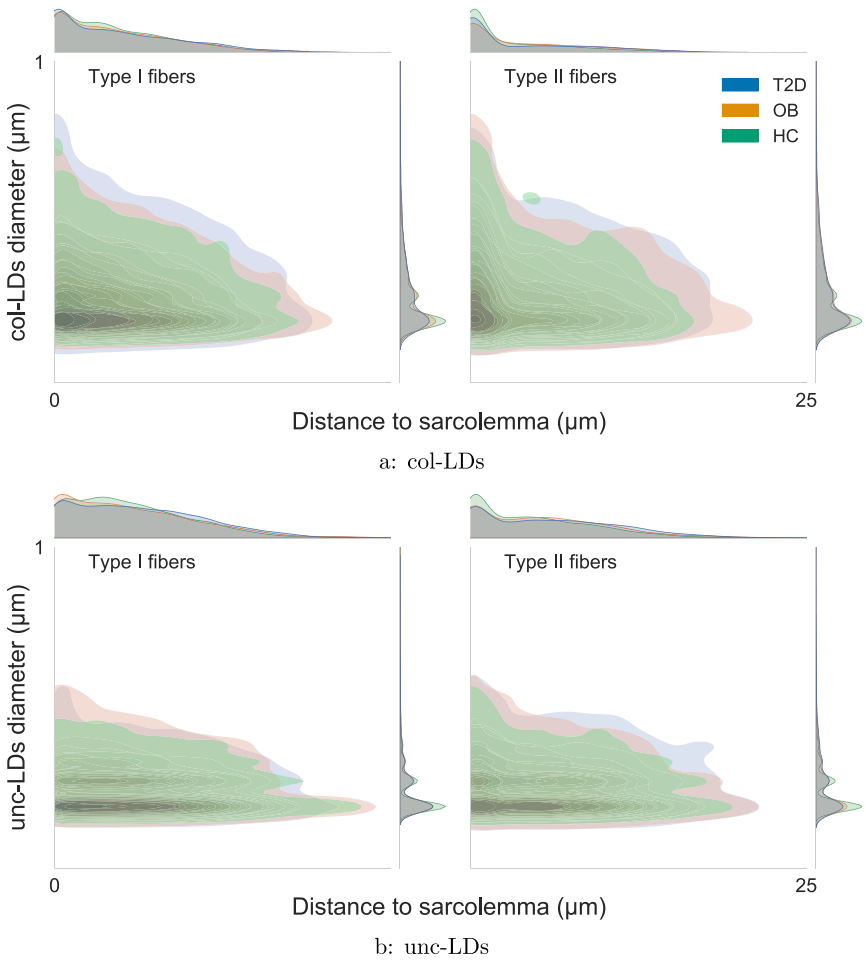


**Fig. 5.** Bivariate kernel density estimation between diameter and distance to sarcolemma of a) col-LDs and b) unc-LDs. From each fiber type and particle type, 500 LDs per subject were randomly selected into a pool representing each group, then from each pool, 3000 LDs were randomly selected to generate the present figure.

### *3.5. Correlations*

We observed a mild positive correlation between the diameter of unc-LDs and blood glucose levels in T2D only, albeit without reaching significance and with no fiber type differences ($\rho = 0.56$, $P = 0.093$ for type I fibers and $\rho = 0.51$, $P = 0.13$ for type II fibers) as seen in Supplement A.1.

Furthermore, we found strong negative correlations between fat percentage and PLIN5 area fraction in HC only (Fig. 6 b), especially in type I fibers (P= 0.002), where PLIN5 abounds.

Interestingly, when testing against $VO_2$ max, we found a strong and significant correlation ($\rho = 0.76$, $P = 0.01$) for unc-LDs in type II fibers of T2D only (Fig. 7b).

## 4. Discussion

### *4.1. Overview*

In this study we examined IMCL, namely area fraction, subcellular localization and size of LDs in different fiber types of obese, type II diabetic and healthy individuals. Additionally, we looked at the association of each of these LDs with PLIN5 across the groups. Amongst the three distinct profiles, T2D and HC were, as expected, the more contrasting ones.

Our main findings were that T2D have increased IMCL uncoated with PLIN5 in type II fibers, mainly in the form of larger LDs in inner regions of the cells. Unlike HC, T2D does not show a decreased area fraction of unc-LDs in type II fibers in comparison to type I fibers (Fig. 2c). This seems to originate from significantly larger unc-LDs, which indeed, were larger in type II than in type I fibers of T2D (Fig. 3c). In normal physiological conditions, type II fibers are expected to have a lower amount of IMCL, as they are known to have a lower oxidative capacity when compared to type I fibers (Malenfant et al., 2001). Possible physiological impacts of this phenomenon remain to be shown.

Equally expected Shaw et al. (2020), is the significantly increased PLIN5 area fraction in type I versus type II fibers, which we observed in every group. In fact, this partially explains the increased col-LDs area fraction in type I fibers of all groups (Fig. 2b and d). It is known that PLIN5 is a responder to increased IMCL in oxidative tissues like skeletal muscle type I fibers. It seems to have a role in protecting muscle against lipotoxicity, by translocating towards IMCL and thus regulating the access of lipases and co-activators, consequently decreasing, if necessary, the rate of triacylglycerol hydrolysis (MacPherson and Peters, 2015). This mechanism has been suggested as a putative role PLIN5 has in attenuating lipid induced insulin resistance in skeletal muscle (Gemmink et al., 2016). Additionally, PLIN5 deletion has been shown to lead to insulin resistance (Mason et al., 2014b, 2014a). Curiously enough, we have observed a mild positive correlation between PLIN5 area fraction and fat percentage in T2D and OB, while HC showed a clearer but negative correlation ($\rho = -0.94$, $P = 0.002$ for type I fibers and $\rho = 0.78$, $P = 0.041$ for type II fibers) as seen in Fig. 6b and Fig. 7.

We were therefore startled, that despite PLIN5′s increased area fraction in type I fibers of T2D, it did not seem equally or sufficiently present in type II fibers of the same group in order to coat the increased IMCL in that same fiber type. This is represented in Fig. 8, where the most impacting contrast between HC and T2D appears to be in type II

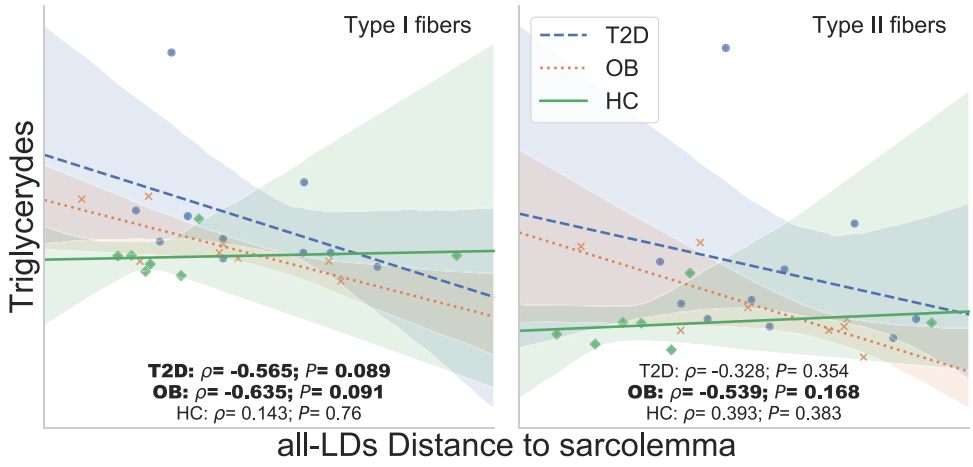


a: All-LDs distance to sarcolemma vs. Triglycerides

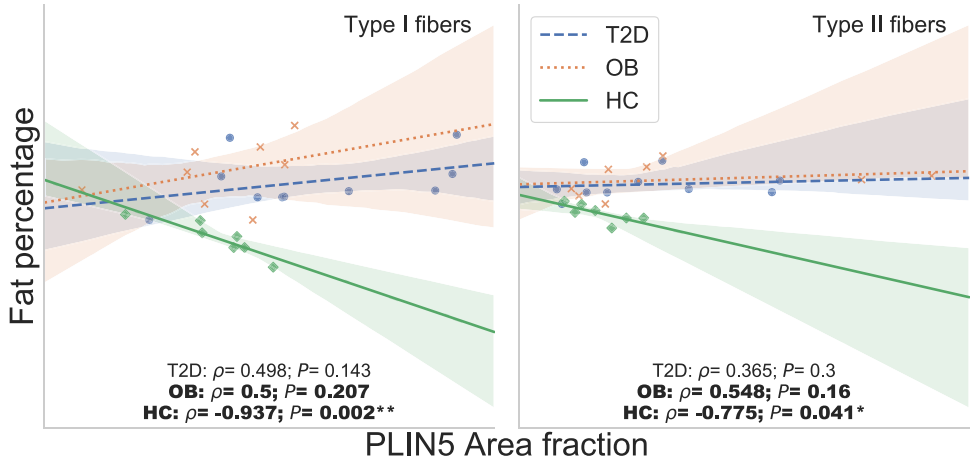


b: PLIN5 area fraction vs. Fat percentage

**Fig. 6.** Linear association with systemic lipids. Between a) Triglycerides and all-LDs distance to sarcolemma; b) PLIN5 area fraction and Fat percentage. Shaded areas show bootstrapped 95% confidence intervals for the fitted regressions. Bold signifies $|\rho| > 0.5$; * $P < 0.05$; ** $P < 0.01$.

fibers, precisely by showing increased amounts of IMCL relatively devoid of PLIN5. Given that PLIN5 area fraction and distance to sarcolemma are not different in T2D type II fibers in comparison to HC, it seems likely that the internalized unc-LDs originate from excess IMCL in general rather than from a diminished presence of PLIN5.

### 4.2. LD size

We observed that not only all-LDs are larger in T2D than in HC, but also that the largest droplets in both fiber types are coated with PLIN5 (Fig. 3b and Fig. 5a). In accordance, while this manuscript was being prepared, another group has observed that the largest LDs were more extensively coated with PLIN5 in T2D versus athletes (Gemmink et al., 2021). Like in our study, others have observed larger LDs in type II versus type I fibers within T2D, as well as in T2D versus healthy individuals (Koh et al., 2018; Daemen et al., 2018). However, as far as we know, this is the first study demonstrating that a notable portion of these larger droplets in type II fibers is not coated with PLIN5 in T2D, which is clearly contrasting with HC and therefore, likely not physiological (Fig. 3c).

It is important to reinforce the notion that large col-LDs are metabolically active IMCL, which by being close to the cell membrane, are close to higher densities of mitochondria, enzymes and chaperones, and consequently, more actively hydrolyzing tryacylglycerol into fatty acids or, depending on cell needs, esterifying incoming fatty acids into triacylglycerol. It is therefore, not too surprising that col-LDs tend to be larger. This begs the question, what is the role or impact of enlarged unc-LDs?

### 4.3. Localization of large unc-LDs in type II fibers

We measured the distance of each lipid droplet towards the sarcolemma and found that HC, in average, have more peripheral IMCL in type II than in type I fibers (Fig. 4a). This is somewhat expectable, as type II fibers are less equipped to internalize and process fatty acids (Bonen et al., 1998). Additionally, we observed that not only T2D did not reveal the same fiber type differences as HC, but actually showed type II fibers with more internalized IMCL than the same fiber type in HC (Fig. 4). Previous research as shown that increased IMCL in T2D and OB individuals is at least partially explained by an increased ability to transport and internalize fatty acids (Bonen et al., 2004).

Subcellular localization of IMCL has been studied in similar populations before, and while some studies might have shown concurring results to ours (Van Loon et al., 2004), the relationship between the localization of different sub-populations of LDs and insulin resistance seems far from fully understood. For instance, by means of electron microscopy, type 2 diabetic individuals were shown to possess higher relative amounts of subsarcolemmal IMCL, which in turn, correlated to

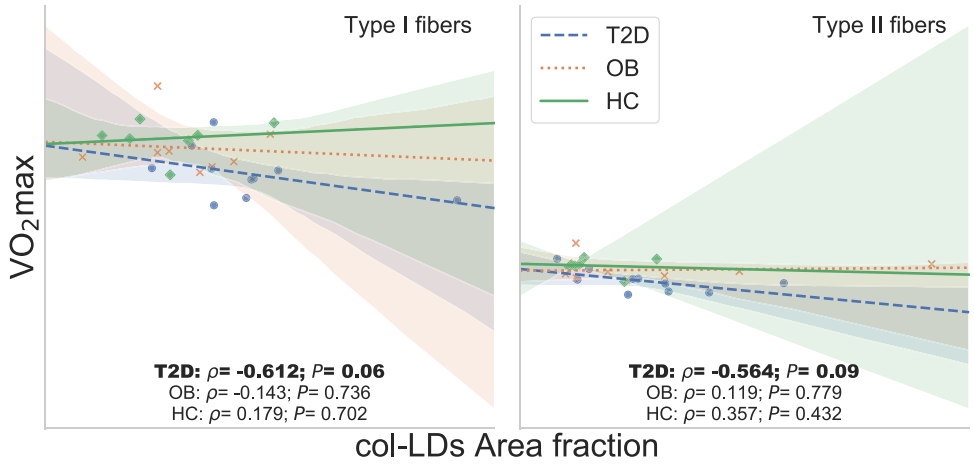


a: col-LDs diameter vs. $VO_2$ max

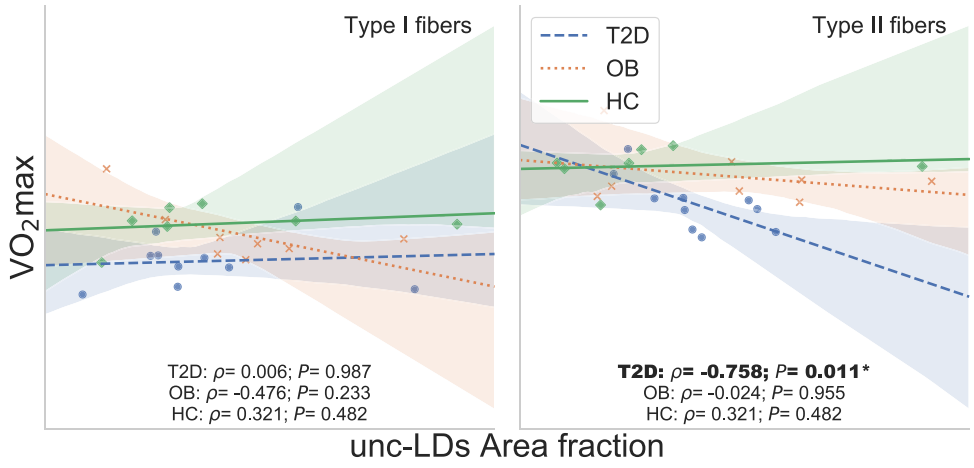


b: unc-LDs diameter vs. $VO_2$ max

**Fig. 7.** Linear association with $VO_2$ max. Between $VO_2$ max and area fraction of a) col-LDs and b) unc-LDs. Shaded areas show bootstrapped 95% confidence intervals for the fitted regressions. Bold signifies $|\rho| > 0.5$; * $P < 0.05$.

insulin resistance (Nielsen et al., 2010). Such results are not necessarily conflicting, as the aforementioned study compared type 2 diabetic with BMI matched obese individuals and endurance athletes. Furthermore, both methods have well known contrasting advantages and disadvantages regarding image resolution and total area sampled, and therefore might not be measuring the same precise physical phenomena. In this study we refrained from using terms like “subsarcolemmal" and “intramyofibrillar", as admittedly, we cannot resolve such regions with confidence. Instead, we measured every detectable LD from hundreds of cells, classified them according to their association with PLIN5 and plotted their distribution.

Despite all-LDs being closer to the membrane in HC type II fibers, subcellular localization of both col-LDs and PLIN5 pools did not differ between HC and T2D (Fig. 4d). However, just like all-LDs, unc-LDs were significantly more internalized in T2D type II fibers versus the same fiber type of HC (Fig. 4c). This led us to suspect that more and larger LDs were left uncoated of PLIN5 in inner regions of T2D type II fibers. We therefore decided to specifically investigate the size of these more internalized unc-LDs, and as suspected, T2D had an important portion of enlarged unc-LDs in inner regions of type II fibers (Fig. 5).

### 4.4. Conclusions

These results point to a novel characteristic in insulin resistant skeletal muscle physiology, i.e., type II fibers are abnormally flooded with large LDs unattended by PLIN5. The importance of this discovery is yet to be completely assessed, it could become paramount and should pave for future research exploring the link between this phenomenon and insulin resistance.

Together with the fact that type II fibers have poorer machinery to process and hydrolyze triacyglycerol, it becomes tempting to hypothesize that, such increased amounts of IMCL uncoated with PLIN5 in type II fibers could be mechanistically associated with skeletal muscle insulin resistance.

Moreover, we observed that larger unc-LDs correlate positively with blood glucose levels in T2D only, although weakly and with no apparent fiber type differences (Supplement A.1). As often associated to insulin resistance (Leite et al., 2009; Morinder et al., 2009), we further observed $VO_2$ max strongly correlate with unc-LDs area fraction in type II fibers of T2D (Fig. 7b).

Whether these forsaken large droplets are downstream or upstream the insulin resistance pathway, is something that cannot be answered with this study. While the failure of PLIN5 in coating LDs may lead to insulin resistance, such mechanism seems to require some degree triacyglycerol hydrolysis by lipases such as ATGL or HSL and presence of mitochondria (Watt, 2009; Bruce et al., 2007; Machann et al., 2004; MacPherson and Peters, 2015), most of which tend to be closer to the sarcolemma (Mason et al., 2014a, 2014b).

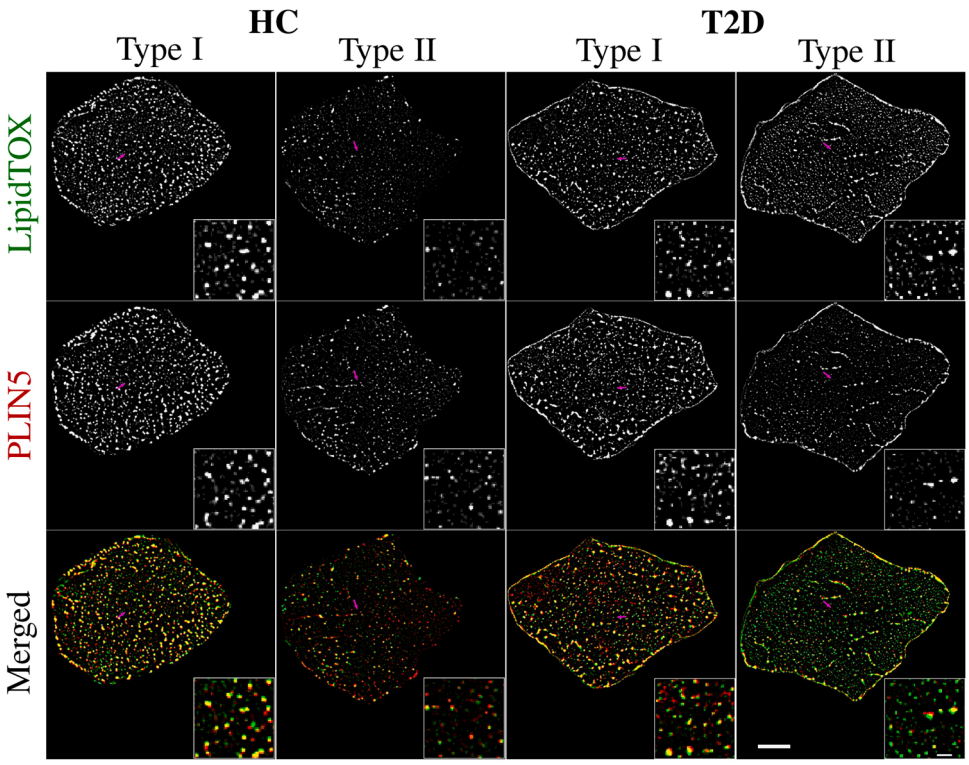


**Fig. 8.** Representative image of IMCL and PLIN5 in different fiber types. Note greener type II fibers in T2D, depicting increased IMCL (green) unattended by PLIN5 (red). Small boxes correspond to the area pointed by magenta arrows. Large bar = 10 $\mu$m; small bar = 2 $\mu$m.

In the future it would be interesting to repeat similar setups using additional markers, like the lipases mentioned above and the CGI-58 co-activator, which hydrolyzing activity has been shown to be inhibited upon PLIN5′s presence (Granneman et al., 2009, 2011; Wang et al., 2011). It will be important to evaluate any possible interaction between such hydrolyzing agents and the sub-population of large and internalized unc-LDs identified in this study.

### 4.5. *Limitations, strengths and implications*

Care should be taken when interpreting light microscopy data from muscle sections. Even if the imaging equipment plus processing techniques are optimal and the known resolution limit is reached, many if not most LDs will remain undetected. Better resolution could be achieved with electron microscopy, but there would be a significant trade-off in sampling area. Another inherent limitation of such methods concerns the representability offered by a thin section, from a small biopsy of a given specific muscle, from a small number of subjects, at a given time. We believe some of our results could reveal clearer and more significant with a larger number of statistical cases. To add to the latter, we acknowledge the fact that all but one T2D subjects were medicated, which could have an impact on intramyocellular PLIN5 (Minnaard et al., 2009). Moreover, like often in literature, we made a dual classification of fiber types, which is likely too simplistic to represent the real and large spectrum of fibers present in skeletal muscle. A final note on the limitations of this study should be given to the fact that for sake of comparability, only male subjects were studied, although there are known differences between genders regarding this topic.

Nevertheless, thorough image processing techniques grant us confidence in data validity, while robust data analysis methods allowed us to measure and visualize the relationships between size, localization and association of LDs with PLIN5 between groups. Thus, we are able to report a clear and novel pattern, emerging from the increased unc-LDs in inner regions of type II fibers of T2D.

Our observations provide clues for future directions concerning the study of lipid droplets and PLIN5 in skeletal muscle insulin resistance. We believe it is important to continue investigating the physiology of different lipid droplet sub-populations, specifically, enlarged unc-LDs in inner regions of type II fibers.

## Funding

This study was supported by the Academy of Finland (grant 132987 and 298875) and Fundação para a Ciência e a Tecnologia (FCT, Portugal) under grant UIDB/04111/2020 (COPELABS). The author Vasco Fachada acknowledges his FCT grant SFRH/BD/68308/2010.

## Conflict of interest

The authors declare that there are no conflicts of interest associated with this manuscript.

## Author contribution statement

VF interpreted the data and wrote the manuscript. HK, UK, PR and VF designed the study. NF, HK and UK contributed to writing the manuscript. Immunohistochemistry and microscopy were carried by VF and PR. Bioinformatics was carried by VF, NF and TT. All authors read and approved the final version of the manuscript.

## Appendix A. Supporting information

Supplementary data associated with this article can be found in the online version at doi:10.1016/j.acthis.2022.151869.

## References

Anon, 2020. T. pandas development team, pandas-dev/pandas: Pandas (Feb. 2020). 10.5281/zenodo.3509134.

Bickel, P.E., Tansey, J.T., Welte, M.A., 2009. Pat proteins, an ancient family of lipid droplet proteins that regulate cellular lipid stores. Biochim. Biophys. Acta (BBA)

Mol. Cell Biol. Lipids 1791 (6), 419–440 (lipid Droplets as dynamic organelles connecting influx, efflux and storage of lipids).
Bonen, A., Luiken, J., Liu, S., Dyck, D., Kiens, B., Kristiansen, S., Turcotte, L., Van Der Vusse, G., Glatz, J., 1998. Palmitate transport and fatty acid transporters in red and white muscles. Am. J. Physiol. Endocrinol. Metab. 275 (3), E471–E478.
Bonen, A., Parolin, M.L., Steinberg, G.R., Calles-Escandon, J., Tandon, N.N., Glatz, J.F., Luiken, J.J., Heigenhauser, G.J., Dyck, D.J., 2004. Triacylglycerol accumulation in human obesity and type 2 diabetes is associated with increased rates of skeletal muscle fatty acid transport and increased sarcolemmal fat/cd36. FASEB J. 18 (10), 1144–1146.
Bruce, C.R., Brolin, C., Turner, N., Cleasby, M.E., van der Leij, F.R., Cooney, G.J., Kraegen, E.W., 2007. Overexpression of carnitine palmitoyltransferase i in skeletal muscle in vivo increases fatty acid oxidation and reduces triacylglycerol esterification. Am. J. Physiol. Endocrinol. Metab. 292 (4), E1231–E1237.
Coen, P.M., Dubé, J.J., Amati, F., Stefanovic-Racic, M., Ferrell, R.E., Toledo, F.G., Goodpaster, B.H., 2009. Insulin resistance is associated with higher intramyocellular triglycerides in type i but not type ii myocytes concomitant with higher ceramide content. Diabetes.
Costes, S.V., Daelemans, D., Cho, E.H., Dobbin, Z., Pavlakis, G., Lockett, S., 2004. Automatic and quantitative measurement of protein-protein colocalization in live cells. Biophys. J. 86 (6), 3993–4003.
Daemen, S., Gemmink, A., Brouwers, B., Meex, R.C., Huntjens, P.R., Schaart, G., Moonen-Kornips, E., Jörgensen, J., Hoeks, J., Schrauwen, P., Hesselink, M.K., 2018. Distinct lipid droplet characteristics and distribution unmask the apparent contradiction of the athlete's paradox. Mol. Metab. 17, 71–81. https://doi.org/10.1016/j.molmet.2018.08.004. ⟨https://www.sciencedirect.com/science/article/pii/S2212877818307415⟩.
Gemmink, A., Bosma, M., Kuijpers, H.J., Hoeks, J., Schaart, G., van Zandvoort, M.A., Schrauwen, P., Hesselink, M.K., 2016. Decoration of intramyocellular lipid droplets with plin5 modulates fasting-induced insulin resistance and lipotoxicity in humans. Diabetologia 59 (5), 1040–1048.
Gemmink, A., Daemen, S., Brouwers, B., Hoeks, J., Schaart, G., Knoops, K., Schrauwen, P., Hesselink, M.K., 2021. Decoration of myocellular lipid droplets with perilipins as a marker for in vivo lipid droplet dynamics: a super-resolution microscopy study in trained athletes and insulin resistant individuals. Biochim. Biophys. Acta (BBA) Mol. Cell Biol. Lipids 1866 (2), 158852. https://doi.org/10.1016/j.bbalip.2020.158852. ⟨https://www.sciencedirect.com/science/article/pii/S1388198120302444⟩.
Goodpaster, B.H., Wolf, D., 2004. Skeletal muscle lipid accumulation in obesity, insulin resistance, and type 2 diabetes. Pediatr. Diabetes 5 (4), 219–226.
Goodpaster, B.H., He, J., Watkins, S., Kelley, D.E., 2001. Skeletal muscle lipid content and insulin resistance: evidence for a paradox in endurance-trained athletes. J. Clin. Endocrinol. Metab. 86 (12), 5755–5761.
Granneman, J.G., Moore, H.-P.H., Krishnamoorthy, R., Rathod, M., 2009. Perilipin controls lipolysis by regulating the interactions of ab-hydrolase containing 5 (abhd5) and adipose triglyceride lipase (atgl). J. Biol. Chem. 284 (50), 34538–34544.
Granneman, J.G., Moore, H.-P.H., Mottillo, E.P., Zhu, Z., Zhou, L., 2011. Interactions of perilipin-5 (plin5) with adipose triglyceride lipase. J. Biol. Chem. 286 (7), 5126–5135.
Harris, C.R., Millman, K.J., van der Walt, S.J., Gommers, R., Virtanen, P., Cournapeau, D., Wieser, E., Taylor, J., Berg, S., Smith, N.J., Kern, R., Picus, M., Hoyer, S., van Kerkwijk, M.H., Brett, M., Haldane, A., FernándezdelRío, J., Wiebe, M., Peterson, P., Gérard-Marchant, P., Sheppard, K., Reddy, T., Weckesser, W., Abbasi, H., Gohlke, C., Oliphant, T.E., 2020. Array programming with NumPy. Nature 585, 357–362. https://doi.org/10.1038/s41586-020-2649-2.
Hunter, J.D., 2007. Matplotlib: a 2d graphics environment. Comput. Sci. Eng. 9 (3), 90–95. https://doi.org/10.1109/MCSE.2007.55.
Koh, H.-C.E., Ørtenblad, N., Winding, K.M., Hellsten, Y., Mortensen, S.P., Nielsen, J., 2018. High-intensity interval, but not endurance, training induces muscle fiber type-specific subsarcolemmal lipid droplet size reduction in type 2 diabetic patients. Am. J. Physiol. Endocrinol. Metab. 315 (5), E872–E884.
Leite, S.A., Monk, A.M., Upham, P.A., Chacra, A.R., Bergenstal, R.M., 2009. Low cardiorespiratory fitness in people at risk for type 2 diabetes: early marker for insulin resistance. Diabetol. Metab. Syndr. 1 (1), 1–6.
LeLay, S., Dugail, I., 2009. Connecting lipid droplet biology and the metabolic syndrome. Prog. Lipid Res. 48 (3–4), 191–195.
Machann, J., Häring, H., Schick, F., Stumvoll, M., 2004. Intramyocellular lipids and insulin resistance. Diabetes Obes. Metab. 6 (4), 239–248.
MacPherson, R.E., Peters, S.J., 2015. Piecing together the puzzle of perilipin proteins and skeletal muscle lipolysis. Appl. Physiol. Nutr. Metab. 40 (7), 641–651. https://doi.org/10.1139/apnm-2014-0485.
Malenfant, P., Joanisse, D., Theriault, R., Goodpaster, B., Kelley, D., Simoneau, J., 2001. Fat content in individual muscle fibers of lean and obese subjects. Int. J. Obes. 25 (9), 1316–1321.
Mason, R., Meex, R., Russell, A., Canny, B., Watt, M., 2014. Cellular localization and associations of the major lipolytic proteins in human skeletal muscle at rest and during exercise. PLoS One 9, e103062. https://doi.org/10.1371/journal.pone.0103062.
Mason, R.R., Watt, M.J., 2015. Unraveling the roles of plin5: linking cell biology to physiology. Trends Endocrinol. Metab. 26 (3), 144–152.
Mason, R.R., Mokhtar, R., Matzaris, M., Selathurai, A., Kowalski, G.M., Mokbel, N., Meikle, P.J., Bruce, C.R., Watt, M.J., 2014. Plin5 deletion remodels intracellular lipid composition and causes insulin resistance in muscle. Mol. Metab. 3 (6), 652–663.
Minnaard, R., Schrauwen, P., Schaart, G., Jorgensen, J.A., Lenaers, E., Mensink, M., Hesselink, M.K., 2009. Adipocyte differentiation-related protein and oxpat in rat and human skeletal muscle: involvement in lipid accumulation and type 2 diabetes mellitus. J. Clin. Endocrinol. Metab. 94 (10), 4077–4085.
Morinder, G., Larsson, U.E., Norgren, S., Marcus, C., 2009. Insulin sensitivity, vo2max and body composition in severely obese swedish children and adolescents. Acta Paediatr. 98 (1), 132–138.
Moro, C., Bajpeyi, S., Smith, S.R., 2008. Determinants of intramyocellular triglyceride turnover: implications for insulin sensitivity. Am. J. Physiol. Endocrinol. Metab. 294 (2), E203–E213.
Nielsen, J., Mogensen, M., Vind, B.F., Sahlin, K., Højlund, K., Schrøder, H.D., Ørtenblad, N., 2010. Increased subsarcolemmal lipids in type 2 diabetes: effect of training on localization of lipids, mitochondria, and glycogen in sedentary human skeletal muscle. Am. J. Physiol. Endocrinol. Metab. 298 (3), E706–E713.
Nissinen, T.A., Hentilä, J., Fachada, V., Lautaoja, J.H., Pasternack, A., Ritvos, O., Kivelä, R., Hulmi, J.J., 2021. Muscle follistatin gene delivery increases muscle protein synthesis independent of periodical physical inactivity and fasting. FASEB J. 35 (3), e21387.
Russell, A., 2004. Lipotoxicity: the obese and endurance-trained paradox. Int. J. Obes. 28 (4), S66–S71.
Schneider, C.A., Rasband, W.S., Eliceiri, K.W., 2012. Nih image to imagej: 25 years of image analysis. Nat. Methods 9 (7), 671–675.
Seabold, S., Perktold, J., 2010. statsmodels: econometric and statistical modeling with python. In: 9th Python in Science Conference, 2010.
Shaw, C.S., Jones, D.A., Wagenmakers, A.J., 2008. Network distribution of mitochondria and lipid droplets in human muscle fibres. Histochem. Cell Biol. 129 (1), 65–72.
Shaw, C.S., Sherlock, M., Stewart, P.M., Wagenmakers, A.J., 2009. Adipophilin distribution and colocalisation with lipid droplets in skeletal muscle. Histochem. Cell Biol. 131 (5), 575–581.
Shaw, C.S., Swinton, C., Morales-Scholz, M.G., McRae, N., Erftemeyer, T., Aldous, A., Murphy, R.M., Howlett, K.F., 2020. Impact of exercise training status on the fiber type-specific abundance of proteins regulating intramuscular lipid metabolism. J. Appl. Physiol. 128 (2), 379–389.
van Loon, L.J., Goodpaster, B.H., 2006. Increased intramuscular lipid storage in the insulin-resistant and endurance-trained state. Pflüg. Arch. 451 (5), 606–616.
Van Loon, L.J., Koopman, R., Manders, R., van der Weegen, W., van Kranenburg, G.P., Keizer, H.A., 2004. Intramyocellular lipid content in type 2 diabetes patients compared with overweight sedentary men and highly trained endurance athletes. Am. J. Physiol. Endocrinol. Metab. 287 (3), E558–E565.
Virtanen, P., Gommers, R., Oliphant, T.E., Haberland, M., Reddy, T., Cournapeau, D., Burovski, E., Peterson, P., Weckesser, W., Bright, J., van der Walt, S.J., Brett, M., Wilson, J., Millman, K.J., Mayorov, N., Nelson, A.R.J., Jones, E., Kern, R., Larson, E., Carey, C.J., Polat, İ., Feng, Y., Moore, E.W., VanderPlas, J., Laxalde, D., Perktold, J., Cimrman, R., Henriksen, I., Quintero, E.A., Harris, C.R., Archibald, A.M., Ribeiro, A.H., Pedregosa, F., van Mulbregt, P., 2020. SciPy 1.0 Contributors, SciPy 1.0: fundamental algorithms for scientific computing in Python. Nat. Methods 17, 261–272. https://doi.org/10.1038/s41592-019-0686-2.
Wang, H., Bell, M., Sreenevasan, U., Hu, H., Liu, J., Dalen, K., Londos, C., Yamaguchi, T., Rizzo, M.A., Coleman, R., et al., 2011. Unique regulation of adipose triglyceride lipase (atgl) by perilipin 5, a lipid droplet-associated protein. J. Biol. Chem. 286 (18), 15707–15715.
Waskom, M., 2020. The seaborn development team, mwaskom/seaborn (Sep. 2020). 10.5281/zenodo.592845.
Watt, M.J., 2009. Storing up trouble: does accumulation of intramyocellular triglyceride protect skeletal muscle from insulin resistance? Clin. Exp. Pharmacol. Physiol. 36 (1), 5–11.
Wolins, N.E., Quaynor, B.K., Skinner, J.R., Tzekov, A., Croce, M.A., Gropler, M.C., Varma, V., Yao-Borengasser, A., Rasouli, N., Kern, P.A., et al., 2006. Oxpat/pat-1 is a ppar-induced lipid droplet protein that promotes fatty acid utilization. Diabetes 55 (12), 3418–3428.